Streaming potential/current measurement system for investigation of liquids confined in extended-nanospace

Kyojiro Morikawa,[a] Kazuma Mawatari,[a] Masaru Kato,[b] Takehiko Tsukahara[c] and Takehiko Kitamori*[a]

Received 13th August 2009, Accepted 21st December 2009
First published as an Advance Article on the web 20th January 2010
DOI: 10.1039/b916776e

The extended-nanospace, a space on the scale of 10^1–10^3 nm, is mostly unexplored due to the lack of sufficient experimental technology. Recently, the research of liquid properties in the extended-nanospace has gathered much interest, because the behavior of water molecules in this space is between that of liquid-like bulk phase water molecules and single molecules. Due to the large surface-to-volume ratio in the channel, the surface charge of the wall directly affects the water structure and ion distribution. The streaming potential/current measurement method, which is used to evaluate surface states directly, is an important and useful method to investigate the liquid properties. In this paper, we report a new method for measuring the streaming potential/current in size-controlled 2D extended-nanospace on glass substrate. Nano-in-microfluidic systems were fabricated on fused-silica glass substrates, and the liquid was air-driven using a pressure controller. An equivalent circuit of the detection system was designed to selectively detect the potential and current in the extended-nanospace. The basic measurement principle was verified using several different experiments. The absolute values obtained for the potential and current were also compared with the theoretical values for various channel sizes (360–1650 nm), and good agreement was observed for micrometre-scale channels. This technique will be valuable for the investigation of chemistry and fluidics in the extended-nanospace.

Introduction

Integrated micro-chemical systems have been developed as high speed, functional and compact instrumentation in the fields of chemical analysis, synthesis, microbiology and related technological fields. A number of practical microsystems have been reported in analytical fields.[1–5]

Recently, the target for micro-nano-integration is downscaling to the 10^1–10^3 nm scale, referred to as extended-nanospace.[6] Fluidic systems in this space are distinguished from those in the 10^0–10^1 nm scale nanospace in conventional nanotechnology. The extended-nanospace bridges the molecular space between single molecules and the bulk phase. Liquid properties in this space were unexplored due to the lack of appropriate research tools.

We have worked on basic research tools for the two-dimensional (2D) extended-nanospace. For example, we have developed nano-in-microchips with size-controlled extended-nanochannels on glass substrates, pressure-driven fluidic control systems, surface modification methods, and detection technologies.[6–9] The properties of water confined in extended-nanospace were investigated using these methods and various specific liquid properties were clarified.[10] For example, studies on the introduction speed using capillary force and time-resolved fluorescent studies showed that the viscosity and dielectric constant of water in extended-nanospace were different from those in the bulk space.[11] In addition, our recent nuclear magnetic resonance (NMR) relaxation measurements of water confined in the extended-nanospace showed slower intermolecular motion and higher proton mobility in comparison to bulk water. We proposed the proton transfer phase model, in which water molecules are loosely coupled within 50 nm from the surface.[12,13] However, the origin of these specific liquid properties is still unclear. One of the reasons is thought to be the effect of the electric double layer (EDL). As the extended-nanospace is comparable in scale to the EDL, most of the space should consist of the EDL. In addition, the surface-to-volume ratio is extremely high in the extended-nanospace; therefore, the surface charge should have a significant effect on the liquid properties. Then, consideration of the EDL and surface charge is important to clarify the chemistry in the extended-nanospace, especially for a detailed discussion of the proton transfer model.

Streaming potential/current measurements were developed to evaluate the surface state directly. The streaming potential/current measurement method was mainly used for the evaluation of zeta potential in capillaries and membrane surfaces,[14–16] because it is a sensitive electrical detection method that can obtain surface information such as the ion distribution in fluids. In addition, the theory for generation of electric signals with regard to surface conditions has been well established.[17,18] Many theoretical and experimental investigations have been carried out.[19–23] We expect that this method will be an important tool for the analysis of extended-nanospace chemistry. Especially, measurement in size-controlled 2D extended-nanochannel on glass substrate is important to investigate the reported specific liquid properties.

[a]*Department of Applied Chemistry, School of Engineering, The University of Tokyo, 7-3-1 Hongo, Bunkyo, Tokyo, 113-8656, Japan. E-mail: kitamori@icl.t.u-tokyo.ac.jp; Fax: +81 3 5841 6039*
[b]*Graduate School of Pharmaceutical Sciences, The University of Tokyo, 7-3-1 Hongo, Bunkyo, Tokyo, 113-8656, Japan*
[c]*Research Laboratory for Nuclear Reactors, Tokyo Institute of Technology, 2-12-1-N1-34, O-Okayama, Meguro, Tokyo, 152-8550, Japan*

Streaming potential/current measurement methods were conventionally used for measurements in micrometre-sized space and nanopores. Recently, van der Heyden *et al.*[24] established a streaming potential/current measurement method in 1D extended-nanospace. Xie *et al.*[25] reported streaming potential/current measurements in 2D extended-nanospace (nanopore). However, a track-etched nanopore made of polyethylene terephthalate had different diameters at the inlet of the pore and the middle of the pore. Therefore, measurement in a size-controlled 2D extended-nanospace was difficult in addition to the difference of the substrate materials, and the investigation of specific liquid properties in size-controlled 2D extended-nanospace on glass substrate is difficult.

One of the difficulties in the development of such a system in 2D extended-nanospace is fluidic control in the extended-nanospace. External electric fields have been mainly used for introduction of liquid into this space, such as studies of the unique ion behavior under an electric field in a nanochannel.[26] The introduction of fluid to nanopores by electroosmotic flow[27] has been established; however, a pressure introduction method is required for streaming potential/current measurement systems. A conventional chip with a straight channel (reservoir, 1D extended-nanochannel and reservoir in line) complicates liquid injection and exchange and requires a long time (several hours) due to low flow rates in the extended-nanochannel as shown in the system reported by van der Heyden *et al.*[24] We have developed a nano-in-microfluidic control system[6] that uses air-pressure control (MPa order). The system employs a combined micro–nanochannel system (microchannel for injection and extended-nanochannel for measurement) for stable liquid injection, rapid liquid exchange and the prevention of bubble and dust introduction into the extended-nanochannels. This nanofluidic control system was applied for streaming potential/current measurements performed in this investigation. Hydrodynamic and electrostatic conditions are important due to the large pressure drop and high electric resistance in the extended-nanochannels, which in turn lead to small signals which are difficult to detect. For this reason, appropriate channel design is essential.

In this paper, we developed a new method for measuring the streaming potential/current in size-controlled 2D extended-nanospace on glass substrate. An equivalent circuit was designed for streaming potential/current measurement in the extended-nanospace. The measurement system was evaluated with respect to the relationship between signals and applied pressure. The relationship between signals and surface charge was also confirmed. Finally, absolute values of the signals were compared to theoretical values.

Theory

Streaming current and streaming potential

Silanol groups on a glass surface dissociate in an aqueous medium. The surface charge and accumulated counter ions in the proximity of the surface form an EDL. Application of a pressure leads to an ion flow in the EDL. The pressure-driven ion flow in turn generates a streaming current I_S that can be calculated theoretically:[15]

$$I_S = -\frac{\pi a^2 \varepsilon \zeta}{\mu L}\left[1 - \frac{2}{j\kappa a}\frac{J_1(j\kappa a)}{J_0(j\kappa a)}\right]\Delta P \quad (1)$$

where a is the channel radius, ε is the dielectric constant, ζ is the zeta potential, μ is the viscosity, L is the channel length, κ^{-1} is the Debye length, J_0 and J_1 are Bessel functions of zero and first order, respectively, and ΔP is the pressure difference across the channel.

Inside a channel, a streaming current leads to the generation of a potential across the channel, the initial streaming potential. This potential in turn generates a conduction current, I_C, in the opposite direction to the streaming current, which influences the streaming potential. At equilibrium, a current, *i.e.*, $I_S - I_C \approx 0$, and a constant streaming potential, U_S, are present inside the channel. At that time, U_S is described by Ohm's law using I_C and the resistance of the channel:

$$U_S = \frac{\varepsilon \zeta}{\mu K}\left[1 - \frac{2}{j\kappa a}\frac{J_1(j\kappa a)}{J_0(j\kappa a)}\right]\Delta P \quad (2)$$

where K is the electrical conductivity.

Circuit

Fig. 1 shows the electrical circuit applied in our experiment. Extended-nanochannels for measurement are connected *via* microchannels for injection into an electrometer with internal resistance, R_L. The pressure-driven flow acts as a constant-current power supply. The channel sizes are designed hydrodynamically in a way that a larger pressure drop, ΔP, and a much larger resistance channel, R_n, are present in the extended-nanochannels compared to the pressure drop and resistance, R_m, in the microchannels, so that the effect of the microchannels on the power supply is negligible. Therefore, the effect of the power supply of the microchannels on the circuit is omitted.

For the circuit, the following equations for the measured current, I_L, and voltage, V_L, are obtained:

$$I_L = N(I_S - I_C) \quad (3)$$

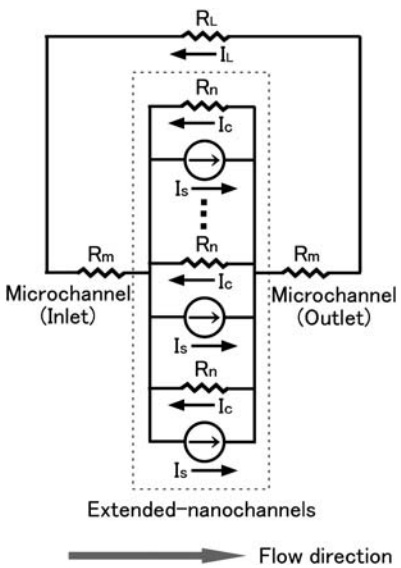

Fig. 1 Illustration of equivalent circuit for streaming potential/current measurement.

$$V_L = I_L R_L = I_C R_n - 2I_L R_m \quad (4)$$

where N is the number of channels. Solving for I_L, we obtain:

$$I_L = NI_S\left(1 + \frac{2R_m + R_L}{R_n/N}\right)^{-1} \quad (5)$$

In the current measurement mode, $I_L = NI_S$ and $I_C \approx 0$ due to the resistance relationship $R_n/N \gg 2R_m \gg R_L$, and I_L is measured.

In the voltage measurement mode, $I_L \approx 0$ due to the resistance relationship $R_L \gg R_n/N \gg 2R_m$. In this condition, eqn (3) results in $I_S - I_C \approx 0$, and V_L can be measured independently of N. I_L and V_L are derived using eqn (1) and (2):

$$I_L = NI_S = -\frac{N\pi a^2 \varepsilon\zeta}{\mu L}\left[1 - \frac{2}{j\kappa a}\frac{J_1(j\kappa a)}{J_0(j\kappa a)}\right]\Delta P \quad (6)$$

$$V_L = I_C R_n = -U_S = -\frac{\varepsilon\zeta}{\mu K}\left[1 - \frac{2}{j\kappa a}\frac{J_1(j\kappa a)}{J_0(j\kappa a)}\right]\Delta P \quad (7)$$

Experimental

The experimental setup is shown in Fig. 2. The fabrication of chips containing extended-nanochannels has been described previously.[6–13] Briefly, extended-nanochannels for measurement were fabricated on a synthetic quartz glass plate by electron beam lithography and plasma etching. At that time, reference channels, the widths of which were larger than the measurement channels, were also fabricated for determination of channel depth by atomic force microscopy (AFM). Microchannels for injection of the sample were etched on another glass slide. The glass plates were combined by thermal fusion bonding. Channel sizes were determined prior to the bonding process using scanning electron microscopy (SEM) for width and AFM depth. A channel cross-sectional shape fabricated by plasma etching was considered as a rectangle.[13] In order to compare channels of similar size with different widths, W, and depths, D, an equivalent diameter, $R = 2a$, was calculated:

$$R = \frac{2DW}{(D + W)} \quad (8)$$

The channel size of the extended-nanochannel was varied for the experiment, while the channel length was kept constant at 400 μm. Sizes of the measurement channels used in measurements were shown in Table 1. The width of the microchannel was

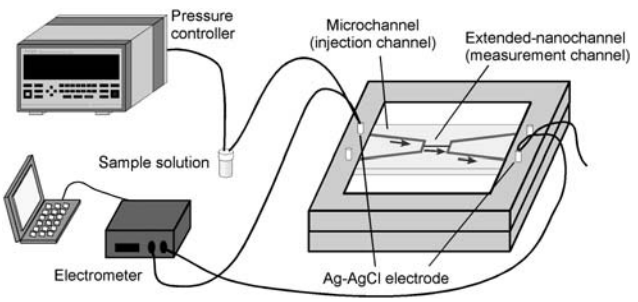

Fig. 2 Schematic illustration of the streaming potential/current measurement system.

Table 1 Sizes and number of the measurement channels

R/nm	W/nm	D/nm	N
580	610	560	1
360	380	350	1
380	380	380	10
360	380	340	30
360	380	350	50
1060	1200	950	1
1650	1580	1730	1

500 μm and the depth was at least 6 μm, and the distance from the inlet to the entrance of the extended-nanochannel as well as the distance from the exit to the outlet was 30 mm. Under these conditions, the microchannel has almost no hydrodynamic and electrical effect on the measurement in the extended-nanochannels. For example, in a single channel with $R = 500$ nm, the pressure drop is estimated to be 99.99629% in the extended-nanochannel and 0.00371% in the microchannel, and the electrical resistance is estimated to be 98.77% in the extended-nanochannel and 1.23% in the microchannel.

Ag–AgCl electrodes fabricated by coating Pt wire with Ag–AgCl paste were connected to the inlet and the outlet of microchannels. Outlets that were not required were closed. Each electrode was connected to an electrometer (Keithley 6514, high impedance of 200 TΩ in voltage measurement mode, Keithley Instruments, Inc., USA). Sample solutions were driven with a pressure controller. The current generated from the inlet to the outlet was measured. The potential at the outlet was measured against the potential at the inlet. Water in all samples was treated with a water purification system composed of reverse osmosis membrane, ion-exchange cylinder, and UV sterilizer (MINIPURE TW-300RU, Nomura Micro Science Co., Ltd., Japan), and had a specific resistivity >18.0 MΩ cm. All experiments were performed at room temperature (20 ± 1 °C).

The zeta potential of glass plates was obtained using a zeta potential meter (ELS8000, Otsuka Electron Co., Ltd., Japan).

Results and discussion

The electric signals were firstly evaluated in relation to the applied pressure to evaluate the fluidic system. Constant-current and voltage values were obtained at an applied constant pressure after equilibrium, as shown in Fig. 3. The signal fluctuation after equilibrium was less than 1% and quite stable. This result verified that constant flow rates were obtained at constant applied pressures. When the applied pressure was increased, the signals were affected by a non-uniform flow, which resulted in disturbed signals. After a while, the current and voltage values also increased and gradually became constant. Although the current values became constant after approximately 1.5 min at each applied pressure, the voltage values required 15 min to equilibrate. This difference in response is derived from the measurement principle in the circuit. The current is measured by the direct detection of I_S with a small electrometer resistance, R_L. On the other hand, the voltage is measured with a large R_L, so that it takes longer to achieve the equilibrium of $I_S - I_C \approx 0$.

A linear relationship between the voltage/current values and applied pressures was obtained after equilibrium as shown in

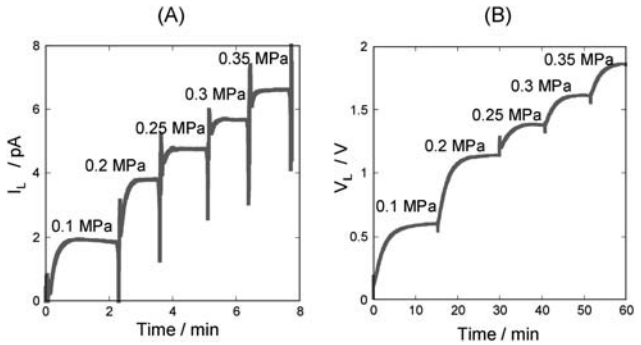

Fig. 3 Streaming potential/current time-course signals at different applied pressures ($R = 580$ nm, sample is pure water): (A) current value and (B) voltage.

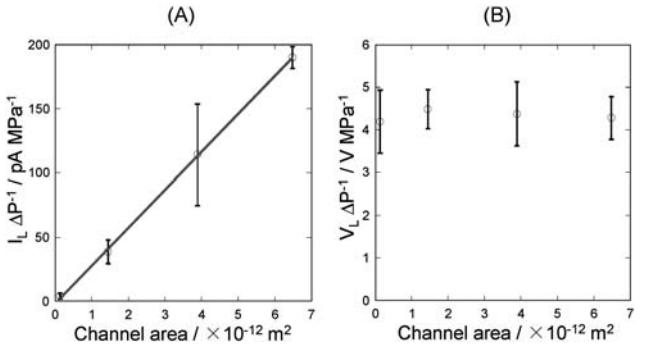

Fig. 5 Dependence on the channel surface area: (A) normalized current and (B) normalized voltage. The sizes and the number of the channels are $R = 360$ nm $\times$ 1, $R = 380$ nm $\times$ 10, $R = 360$ nm $\times$ 30 and $R = 360$ nm $\times$ 50. Sample is pure water.

Fig. 4 (unmodified surface). The current and voltage were proportional to the applied pressure, as expected, which indicates that the flow rate inside the channels was increased according to the pressure increase. For this reason, normalized current values, $I_L \Delta P^{-1}$, and normalized voltage values, $V_L \Delta P^{-1}$, are used in the following discussion. Due to a good linear relationship between voltage/current values and applied pressures in 0.1–0.35 MPa, the values of $I_L \Delta P^{-1}$ and $V_L \Delta P^{-1}$ had less than 1% error in this normalization. Fig. 4 shows the relationship between the electric signals and the surface charge state. On a negatively charged unmodified surface with silanol groups, positive $I_L \Delta P^{-1}$ and $V_L \Delta P^{-1}$ values were obtained, due to cation flow. A positively charged surface was obtained by modification with 3-amino-propyltriethoxysilane (APTES), which resulted in surface amino groups yielding negative $I_L \Delta P^{-1}$ and $V_L \Delta P^{-1}$ values due to anion flow. Therefore, information regarding the surface charge state was reflected by the electric signals obtained using this setup.

In the next experiment, the current and voltage were measured using chips with different total areas in the extended-nano-channels, mostly due to differing channel numbers. According to eqn (6) and (7), $I_L \Delta P^{-1}$ is proportional to the channel area $N\pi a^2$, and $V_L \Delta P^{-1}$ is independent of the channel area, because the Bessel function term is almost negligible for similar channel

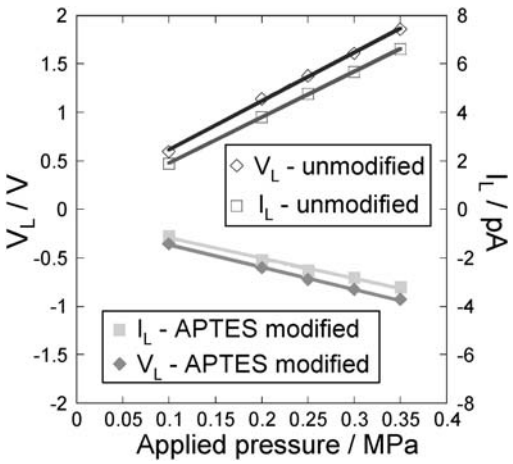

Fig. 4 Voltage and current value as functions of applied pressure in a channel with an unmodified glass surface and an APTES modified glass surface ($R = 580$ nm, sample is pure water).

radius, a. The results were shown in Fig. 5. As above mentioned, $I_L \Delta P^{-1}$ in one experiment had small error. However, the repeated experiment generated larger errors than the signal fluctuations. Then, the error bar ($\pm\sigma$) was included from the three repeated experiments. The value of $I_L \Delta P^{-1}$ increased with increasing channel area, whereas the value of $V_L \Delta P^{-1}$ remained almost the same. These results confirm the applicability of these equations, in addition to the appropriate design of the circuit and channels.

Finally, the dependence of the current and voltage values on the channel size was evaluated using a 10^{-2} M KCl solution. All experiments were performed using single channels ($N = 1$), each with a determined size. Average current and voltage values and errors ($\pm\sigma$) in three experiments were shown in Table 2 It provides a comparison of the obtained current and voltage values in each channel with theoretical values derived from eqn (6) and (7) using the following bulk parameters: $\varepsilon = 7.12 \times 10^{-10}$ F m^{-1}, $\zeta = -5.3 \times 10^{-2}$ V, $\mu = 1.00 \times 10^{-3}$ Pa s, $L = 4.0 \times 10^{-4}$ m, $\kappa^{-1} = 3.05 \times 10^{-9}$ m, $K = 0.128$ S m^{-1}. In the micrometre-sized space, the $I_L \Delta P^{-1}$ values are in accordance with the theoretical values. In contrast, decreased $I_L \Delta P^{-1}$ values were obtained in the extended-nanospace, due to increased viscosity and decreased dielectric constant. On the other hand, decreased $V_L \Delta P^{-1}$ values were obtained in both spaces, due to the increased electrical conductivity (surface conductivity) in the microspace and extended-nanospace. Current values in accordance with the theory (fitted with bulk parameters) were obtained in micro-space, and deviations from the theoretical value were confirmed in the extended-nanospace. Further detailed studies of the evaluation of viscosity, dielectric constant and conductivity using this system are ongoing.

Table 2 Comparison of obtained current and voltage values pressure-normalized I_L and V_L to theoretical streaming current and streaming potential values pressure-normalized I_S and $-U_S$

R/nm	$I_L \Delta P^{-1}$/pA MPa^{-1}	$I_S \Delta P^{-1}$/pA MPa^{-1}	$V_L \Delta P^{-1}$/V MPa^{-1}	$-U_S \Delta P^{-1}$/V MPa^{-1}
580	12.0 ± 1.27	24.4	0.135 ± 0.0118	0.289
1060	76.5 ± 7.77	82.3	0.138 ± 0.00834	0.291
1650	188 ± 47.0	200	0.161 ± 0.0330	0.293

Conclusion

A streaming potential/streaming current measurement system for measurements in size-controlled 2D extended-nanospace on glass substrate was successfully developed for the first time. The fluidic control system and the well-designed micro–nano combination chip enabled sensitive detection of the streaming potential/current in extended-nanospace. Appropriate flow rates at each applied pressure were evaluated by the relationship between the signals and the applied pressure. In addition, information on the surface charge of the extended-nanochannel was correctly obtained with the setup. Theoretical equations and the applied circuit were successfully evaluated by measurements in channels with different surface areas. Finally, the absolute values of the potential and current were compared with theoretical values by varying the sizes of the measurement channel in the setup. In the future, this system will become a useful tool for the investigation of liquid properties in extended-nanospace, in addition to flow rates near the surface and differences in surface composition, for example, due to the adsorption of molecules.

Acknowledgements

This work was supported by JSPS Grant-in-Aid for Specially Promoted Research (21000007).

References

1 D. R. Reyes, D. Iossifidis, P.-A. Auroux and A. Manz, *Anal. Chem.*, 2002, **74**, 2623–2636.
2 D. R. Reyes, D. Iossifidis, P.-A. Auroux and A. Manz, *Anal. Chem.*, 2002, **74**, 2637–2652.
3 K. Sato, M. Tokeshi, T. Odake, H. Kimura, T. Ooi, M. Nakao and T. Kitamori, *Anal. Chem.*, 2000, **72**, 1144–1147.
4 H. Mao, T. Yang and P. S. Cremer, *Anal. Chem.*, 2002, **74**, 379–385.
5 A. Gunther and K. F. Jensen, *Lab Chip*, 2006, **6**, 1487–1503.
6 T. Tsukahara, K. Mawatari, A. Hibara and T. Kitamori, *Anal. Bioanal. Chem.*, 2008, **391**, 2745–2752.
7 E. Tamaki, A. Hibara, H. B. Kim and T. Kitamori, *J. Chromatogr., A*, 2006, **1137**, 256–262.
8 B. Renberg, K. Sato, K. Mawatari, N. Idota, T. Tsukahara and T. Kitamori, *Lab Chip*, 2009, **9**, 1517–1523.
9 R. Kojima, K. Mawatari, B. Renberg, T. Tsukahara and T. Kitamori, *Microchim. Acta*, 2009, **164**, 307–310.
10 A. Hibara, T. Tsukahara and T. Kitamori, *J. Chromatogr., A*, 2009, **1216**, 673–683.
11 A. Hibara, T. Saito, H. B. Kim, M. Tokeshi, T. Ooi, M. Nakao and T. Kitamori, *Anal. Chem.*, 2002, **74**, 6170–6176.
12 T. Tsukahara, A. Hibara, Y. Ikeda and T. Kitamori, *Angew. Chem., Int. Ed.*, 2007, **46**, 1180–1183.
13 T. Tsukahara, W. Mizutani, K. Mawatari and T. Kitamori, *J. Phys. Chem. B*, 2009, **113**, 10808–10816.
14 A. R. Sears and J. N. Groves, *J. Colloid Interface Sci.*, 1978, **65**, 479–482.
15 J. Yang, F. Lu, L. W. Kostiuk and D. Y. Kwok, *J. Micromech. Microeng.*, 2003, **13**, 963–970.
16 A. I. C. Morao, A. M. B. Alves and M. D. Afonso, *J. Membr. Sci.*, 2006, **281**, 417–428.
17 S. Levine, J. R. Marriott, G. Neale and N. Epstein, *J. Colloid Interface Sci.*, 1975, **52**, 136–149.
18 M. S. Chun, T. S. Lee and N. W. Choi, *J. Micromech. Microeng.*, 2005, **15**, 710–719.
19 X. Xuan and D. Sinton, *Microfluid. Nanofluid.*, 2007, **3**, 723–728.
20 C. D. Lorenz and A. Travesset, *Phys. Rev. E: Stat. Phys., Plasmas, Fluids, Relat. Interdiscip. Top.*, 2007, **75**, 061202.
21 Y. Liu, M. Liu, W. M. Lau and J. Yang, *Langmuir*, 2008, **24**, 2884–2891.
22 Y. S. Choi and S. J. Kim, *J. Colloid Interface Sci.*, 2009, **333**, 672–678.
23 C. C. Chang and R. J. Yang, *J. Colloid Interface Sci.*, 2009, **339**, 517–520.
24 F. H. J. van der Heyden, D. Stein and C. Dekker, *Phys. Rev. Lett.*, 2005, **95**, 116104.
25 Y. Xie, X. Wang, J. Xue, K. Jin, L. Chen and Y. Wang, *Appl. Phys. Lett.*, 2008, **93**, 163116.
26 Q. Pu, J. Yun, H. Temkin and S. Liu, *Nano Lett.*, 2004, **4**, 1099–1103.
27 A. Brask, J. P. Kutter and H. Bruus, *Lab Chip*, 2005, **5**, 730–738.